Journal of Applied Electrochemistry **31**: 1195–1202, 2001.

A new technique for online visualization of the electrode surface under electrochemical corrosion processes

J. GARCÍA-ANTÓN, A. IGUAL-MUÑOZ, J.L. GUIÑÓN and V. PÉREZ-HERRANZ
Departamento de Ingeniería Química y Nuclear, E.T.S.I. Industriales, Universidad Politécnica de Valencia, PO Box 22012, E-46071 Valencia, Spain

Received 23 November 2000; accepted in revised form 24 July 2001

Key words: copper, corrosion, lithium bromide, online visualization, stainless steel, surface visualization

Abstract

A new method for the online visualization of corrosion processes has been developed. It relates two techniques, electrochemical studies (potentiodynamic, potentiostatic, chronoamperometric etc.) and image processing. The main advantage of this method is that it is possible to relate the morphological changes of the electrode surfaces to the electrochemical signal measured without disturbing the electrochemical system. The online visualization technique is based on a horizontal electrochemical cell. The cell allows observation of the surface of the electrodes in a horizontal position by means of a triocular microscope–stereoscope assembled to an image acquisition system. The methodology was applied to the study and understanding of the surface changes of a copper and an AISI 316L electrode, respectively, when their potentiodynamic curves were taken in a lithium bromide solution. The corroded area of an AISI 316L electrode was determined by image processing in order to calculate the local current density in a potentiostatic test. The visualization method proposed can be used to gain a better understanding of electrochemical corrosion processes.

1. Introduction

It is generally recognized that the visual observation of corroded surfaces is an essential stage in the identification of corrosion causes [1]. Image analysis is a relevant tool to characterize corrosion processes qualitatively and quantitatively.

Pit growth kinetics have been studied for stainless steels using image analysis [2–4]. Direct correlation between the individual effects on the surface of the specimen and the observed fluctuations of potential and current was established on AISI C1008 carbon steel [5]. The visualization method proposed in this work consists of recording the electrical signal and image acquisition simultaneously. This method allows real-time observation of the electrode surface as it undergoes electrochemical corrosion processes, relating the electrochemical signal to the exact effect of corrosion on the metal. Image data can be analysed in two ways: the first and direct one consists of the real visualization of the surfaces under study. The second analysis comprises the image processing of the images acquired, and includes calculations of the corroded areas, number of pits on a pitted surface, texture analysis, grain shape during an electrochemical assay etc.

Attempts have been made to automatically characterize corrosion (pit formation and cracking) based on visual images [6–8], specifically using texture analysis.

An experimental study of different types of corrosion processes is examined on copper and stainless steel, AISI 316L, respectively, using electrochemical and image processing techniques. The electrodes were immersed in a commercial lithium bromide (LiBr) solution and the electrochemical phenomena produced on their surfaces were observed in real-time. LiBr solution was used in order to continue studies initiated in this medium [9–14] because of its important applications as one of the most efficient absorbents in absorption refrigeration and heating systems.

Different electrochemical techniques, potentiodynamic and potentiostatic scans related to the simultaneously acquired images were employed in order to observe the behaviour of copper and AISI 316L under different conditions.

2. Experimental details

2.1. *Technical specifications of the experimental device*

The experimental arrangement used [15] is shown in Figure 1. It is possible to differentiate two parts: the electrochemical unit and the image acquisition section. The electrochemical system is composed of the data acquisition equipment, a VoltaLAB PGZ301 potentiostat, which registers the electrical signal (current, potential, resistance etc.) obtained from the corrosion

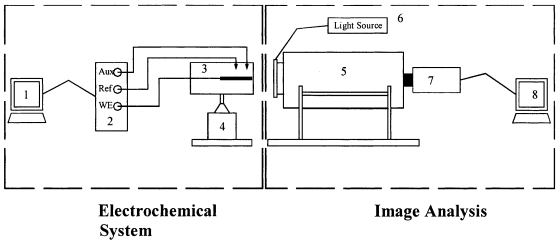

Fig. 1. Scheme of the experimental arrangement: (1) computer (electrical signal acquisition); (2) potentiostat; (3) electrochemical cell; (4) coordinate system; (5) microscope–stereoscope; (6) light source; (7) camera; (8) computer (image acquisition).

processes taking place inside the electrochemical cell. The most important feature of the thermostat cell, designed and constructed in glass [16], is that the visualization of the electrode surface immersed in the solution is possible due to the horizontal orientation of the working electrodes. The cell is fastened with pincers screwed on a coordinate axis system which allows the remaining specimens to be centred and focused during the whole assay. This system also permits adjustment of the electrode position when required. The coordinate system was essential to re-position the electrodes to their original position when they were refocused, and consequently moved.

The second part, corresponding to image acquisition, is formed by a triocular microscope–stereoscope (Nikon SMZ-U) zoom 1:10 and a colour video camera (Sony SSC-C370P), type CCD camera (752×582 pixels) assembled to the optical device. The sensing area of the camera is 6.3 mm $\times$ 4.7 mm with an average resolution of about 10 μm per pixel. For storage in the computer, the analogue signal produced by the camera was digitized with an image acquisition card, and the digital signal obtained was stored in a computer. The acquisition card produces images that have a pixel dimension of 352×240 pixels, captured at a rate of 25 frames per second. It is possible to capture, encode and preview full motion video in MPEG format. The images continuously acquired were then converted into JPEG images. The decision to encode an image into 8 bits was due to several factors, the nature of the image, the image of image processing and the type of analysis to perform. The colour images acquired were composed of three planes of pixels in which each pixel had a red, green and blue intensity, each coded on 8 bit planes. These images were then processed using Visilog 5.2® [17].

2.2. *Experimental conditions and materials*

The materials used were electrolytic copper 99.99 wt % and AISI 316L stainless steel. These metals were machined in order to construct cylindrical electrodes (55 mm high and 8 mm dia.) embedded in Teflon coating, thus having a transverse area of 0.5 cm^2. exposed to corrosion. The electrode surfaces were ground mechanically with emery paper (1000 SiC grit) and polished with alumina (1 μm). They were then rinsed with distilled water and degreased with acetone.

The solution used was a commercial LiBr solution, from FMC Corporation Lithium Division, with a concentration of 55 wt % LiBr (pH 6.95) with Li_2CrO_4 (4.5 wt %) and LiOH (0.0052 wt %) as additives.

Potentiodynamic anodic polarization measurements were generated using a VoltaLAB PGZ301 potentiostat. The potential of the working electrode was measured against a silver–silver chloride (Ag–AgCl 3 M KCl) reference electrode. The auxiliary electrode was platinum (Pt). Reduction of oxygen levels in the solution prior to immersion was accomplished by bubbling nitrogen for 10 min. The inert atmosphere was maintained during the test by passing nitrogen on the solution. Before each polarization, the probe was immersed in the test solution for 1 h at the open-circuit potential (o.c.p.). The average value of the potentials recorded during the last 300 s was accepted as the value of the o.c.p. Once immersed in the solution for 1 h, the sample potential was held at -500 mV for 60 s in order to remove any oxides formed on the metal surface. Then, the electrode potential was scanned from -500 mV vs Ag/AgCl to 1000 mV vs Ag/AgCl at 0.5 mV s^{-1}. Temperature was kept at 25 °C during the tests.

The potentiostatic test consisted of imposing a potential of 50 mV on the AISI 316L for one hour, after immersion at 0 mV for an hour. The current data were recorded during the immersion time.

3. Results

3.1. *Potentiodynamic test of a copper electrode*

The potentiodynamic curve is shown in Figure 2. While the potentiostat was measuring the potential and the current signal, the camera was acquiring the image of the electrode surface continuously. The electrode immersed in the commercial LiBr solution initially presented a surface marked by the straight lines corresponding to the polishing process, Figure 3(a). During the first anodic

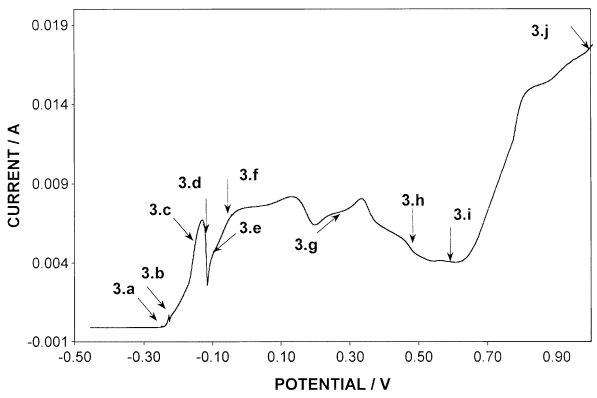

Fig. 2. Potentiodynamic curve of a copper electrode immersed in a commercial LiBr solution. Curve numbers indicate the time when the corresponding images were acquired.

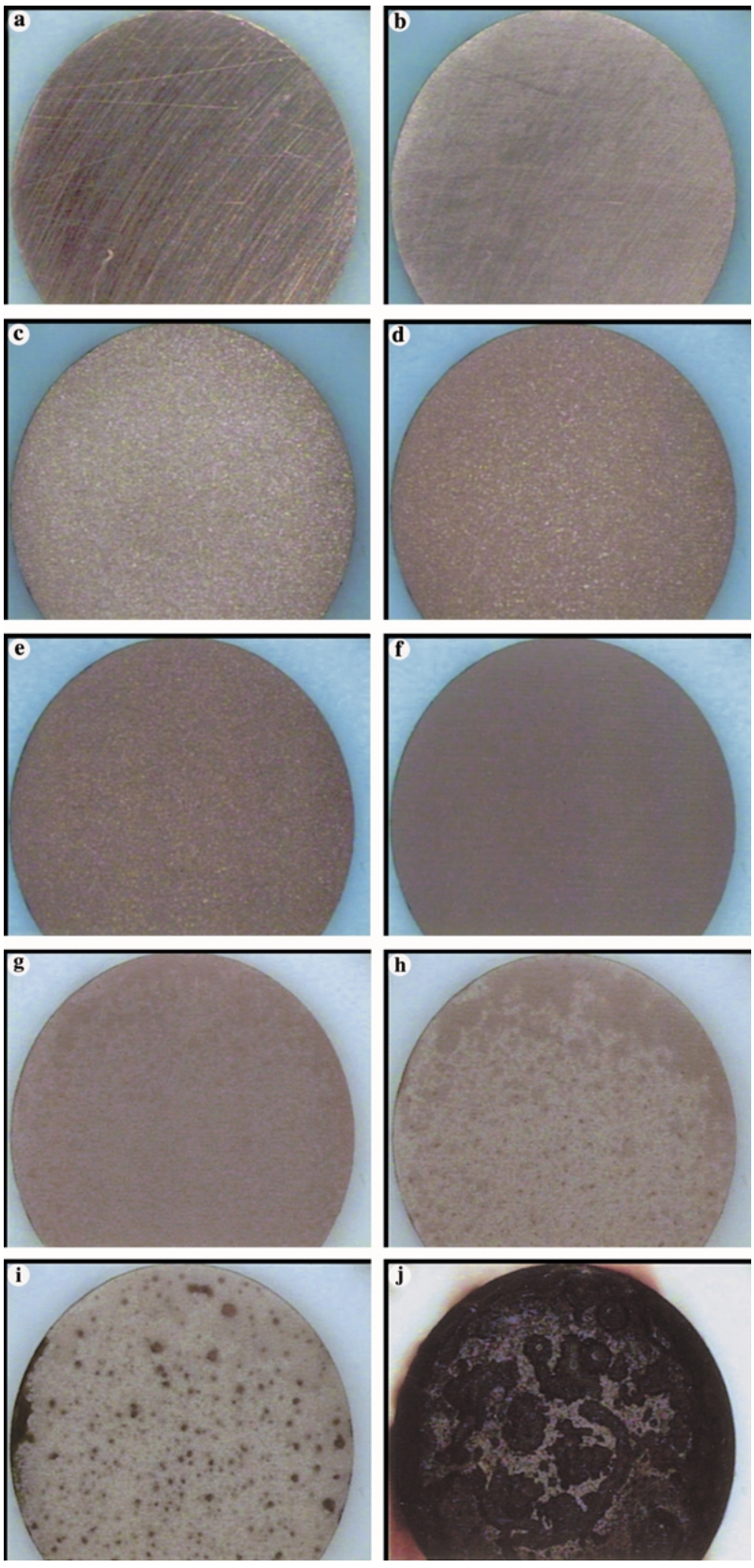

Fig. 3. Images of the copper electrode at different potentials of the potentiodynamic scan in commercial LiBr solution (probe dia. 8 mm): (a) −245 mV, (b) −215 mV, (c) −150 mV, (d) −120 mV, (e) −90 mV, (f) 50 mV, (g) 300 mV, (h) 500 mV, (i) 600 mV and (j) 1000 mV.

peak, the copper electrode underwent a progressive change of appearance; crystal growth occurred on its surface to a maximum at −130 mV. At the beginning of the active phase, the thin Cu_2O film peeled away and the crystals of a new thick phase of Cu_2O began to form [18]. It is possible to observe at −215 mV, Figure 3(b) and at

−150 mV, Figure 3(c), a structure which becomes rougher with increasing potential. The formation of $CuBr_2^-$ complexes could be the reason for the increasing current, by destabilizing the formation of copper oxides and promoting active dissolution of the metal [9]. The copper electrode starts passivating when the surface presents a more homogeneous structure. As can be seen in Figure 3(d) at −120 mV, the surface is then protected by a uniform film with a darker coloration and the regular crystal distribution observed at lower potentials starts decreasing, possibly due to the presence of chromate in the commercial solution. The thin film starts forming at the perimeter and spreads progressively inwards, dislodging the film formed during the active phase. Immediately before the fall from the peak current, the electrode surface loses its polished appearance, becoming dull under the illumination used.

Current reached a minimum at −115 mV and started to increase again when the uniform crystal distribution started to disappear and a greenish film covered the electrode surface. Figure 3(e) and Figure 3(f) taken at −90 mV and 50 mV, respectively, show the attack of copper material with the subsequent product formation on it.

For a wide range of potentials, from 0 mV to around 300 mV, Figure 3(f), the copper surface did not show significant modification. The current oscillated slightly between 7.5 mA and 6.5 mA, the metal corroded at an almost constant rate, and the surface was covered with a uniform brownish film at 0 mV and a greenish product at higher potentials, which altered its homogeneity. The surface became brighter when the potential exceeded 300 mV, Figure 3(g). This current plateau may be attributed to the presence of a CuBr salt film coexisting with a Cu_2O film [19], consistent with the formation of a loosely adherent greenish corrosion product.

At higher potentials, from 350 mV to more than 600 mV, the electrode was again protected by a grey film with some defects. These sites, which are distinguished by their darker coloration, prevent total protection of the metal and allow progressive corrosion of the copper. This phenomenon was observed at the top of the images in Figure 3(h), at 500 mV, and Figure 3(i), at 600 mV. The current fell to values around 4 mA.

When potentials become higher than 620 mV, the protective film started to dissolve and generalized corrosion occurred on the metallic surface. Figure 3(j) shows the preferential corrosion sites identified by the cavities on the copper surface. The brighter areas correspond to a film probably composed of bromide complex salts. At the end of the test, when potential was no longer applied, this film peeled off. The damage was in the form of small and longitudinal cavities.

3.2. *Potentiodynamic test of a stainless steel electrode*

The potentiodynamic curve of the stainless steel AISI 316L in commercial LiBr solution is shown in Figure 4. The specimen was immersed at open circuit for one hour and the scan was started at −250 mV. The photo in Figure 5(a), was taken at the end of the first hour at open circuit and no corrosion was observed.

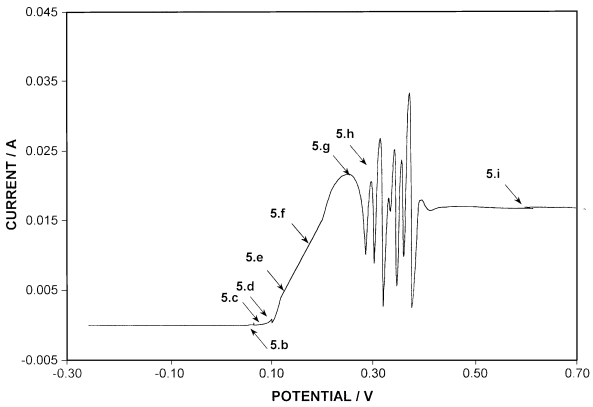

Fig. 4. Potentiodynamic curve of a stainless steel AISI 316L electrode immersed in a commercial LiBr solution. Curve numbers indicate the time when the corresponding images were acquired.

The critical potential [20] was defined as the potential at which a sustained current of 50 μA was established, and was related to corrosion initiation. According to this concept, Figure 5(b) was taken when current reached the threshold of 50 μA (corresponding to a potential of 76 mV). As can be noted in the image, two negligible marks, situated on the crevice between the metal and the Teflon, appeared on the positions equivalent to the 4 h and 8 h of a clock. In contrast, in Figure 5(c), different corrosion sites are clearly visible around the same crevice. This image was acquired at 88 mV when current was 200 μA which could be considered the current threshold to visualize corrosion initiation. Figure 5(d) to Figure 5(g) show how corrosion is initiated around the perimeter of the metal and how it evolves along a vertical direction, from the top to the bottom of the electrode, until covering the whole surface. These images were obtained at 106, 138, 180 and 250 mV, respectively. With the progress of the scanning, surface roughness significantly increased in intensity and exhibited a directional pattern.

The corrosion product, the brownish compound in the images, formed a film on the stainless steel surface, and covered the whole surface at 250 mV, coinciding with the anodic peak in the potentiodynamic curve. Once the total area of the electrode was completely attacked, the same product generated a kind of passivation which caused initially a current decrease, and current oscillations from −285 mV to −400 mV, Figure 5(h) at 300 mV. The current density between 285 mV and 395 mV corresponds to a partly-active–partly-passive state [21, 22].

The preferential corrosion sites correspond with the crevice perimeter during the whole test. When the electrode was completely covered by the brownish product, the film prevented the corrosion product from falling down the electrode, which continued generating and started to accumulate around the perimeter. The

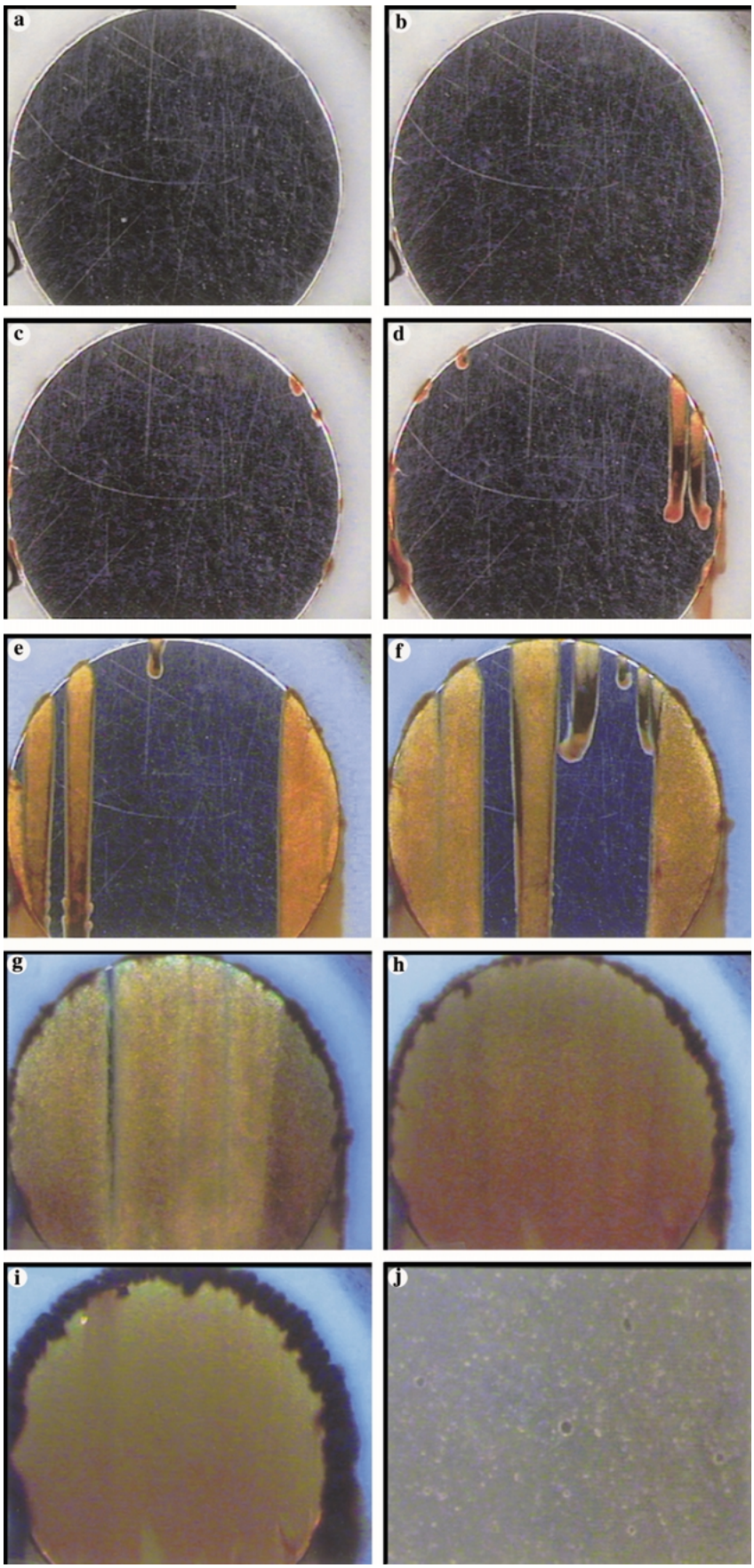

Fig. 5. Images of the AISI 316L electrode at different potentials of the potentiodynamic scan in commercial LiBr solution (probe dia. 8 mm): (a) at o.c.p.; (b) 50 μV; (c) 88 mV; (d) 106 mV; (e) 138 mV; (f) 180 mV; (g) 250 mV; (h) 300 mV; (i) 600 mV and (j) at the end of the test (×75, representing the real area of 0.9 mm × 0.74 mm).

result was the formation of a darker halo concentric to the electrode area which grew more slowly when the potential shifted to more positive values. Figure 5(i) at 600 mV corresponds to the horizontal part of the potentiodynamic curve, when the corrosion attack was established around 15 mA. It was assumed that the electrode was covered by a salt film at all potentials at the limiting-current plateau [21].

At the end of the test the product formed on the stainless steel surface fell off slowly and spread out through the solution. The electrode was then observed, Figure 5(j). Round pits and small grooves were distinguished on its surface with a maximum area of 4.68×10^{-4} mm^2. The sensitivity of this technique allows detection of pits 10 μm in diameter.

3.3. *Potentiostatic test of a stainless steel electrode*

Surface modification of the AISI 316L stainless steel was studied by continuous image acquisition in a commercial LiBr solution at different potentials, 0 mV and 50 mV. The images and the current data were processed every five minutes after the transition period of 10 min, which was not significant.

During the first hour at 0 mV, current oscillated around 0 nA, and the surface did not show any visible modification. The attack started when the potential was increased to 50 mV. The whole surface of the electrode was not attacked at the same rate and at the same instant, thus, the images acquired were processed in order to calculate the area affected and the real current density, which was degrading the stainless steel. The reddish region in Figure 6(a) to Figure 6(c) shows the evolution of the attacked area. The measured current referred to the part of the electrode which was corroding.

The corroded area was calculated according to the following image processing sequence. The colour images were broken down into three sets of primary components, such as Red, Green and Blue (RGB), and processed as any grey-level image. Performing the histogram of each image, it is possible to obtain a quantitative distribution of pixels per grey-level value. The range of grey-level corresponding to the corroded area was selected and the image was binarized. Figure 7 shows an example of a binarized image taken after 40 min of immersion.

Current data and the corroded area are shown in Figure 8. Current density was estimated from the quotient of the measured current and the corroded area at a particular moment. The measured current increased linearly with time while current density decreased exponentially. Although the measured current in the potentiostatic test seemed to indicate that corrosion increased, only the affected area grew and real current density decreased with time (other experiments—potentiodynamic curve of a copper electrode in 3.5 wt % NaCl solution—also demonstrated that the increase in current was related to the attacked area, reaching its maximum current peak when the surface was completely attacked).

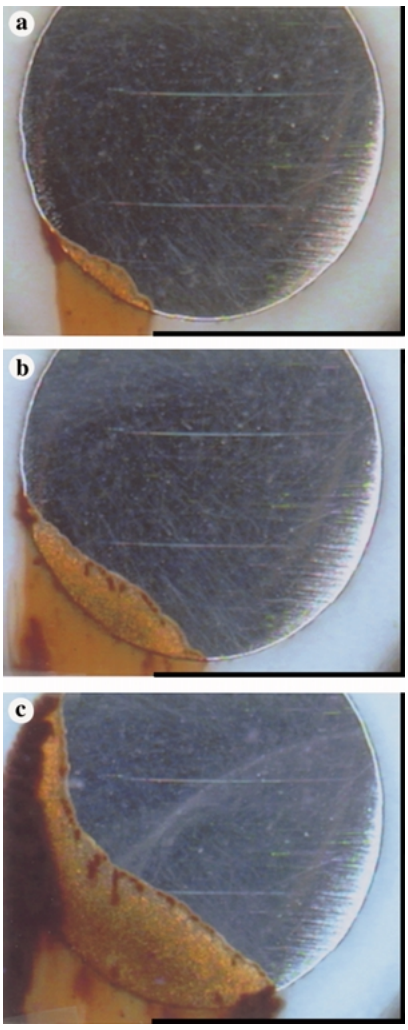

Fig. 6. AISI 316L surface at different times of the immersion in commercial LiBr solution at 50 mV (probe dia. 8 mm): 15 min (corroded area 0.8 mm^2); (b) 30 min (corroded area 3.3 mm^2) and (c) 60 min (corroded area 12.1 mm^2).

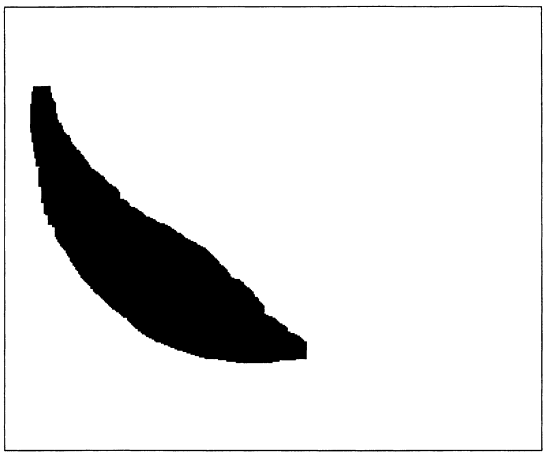

Fig. 7. Binarized image of the corroded area of the AISI 316L after 40 min of immersion.

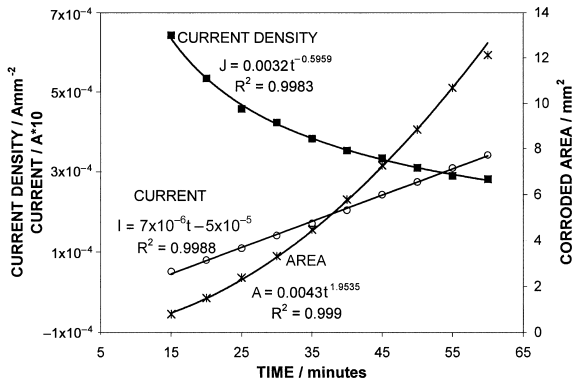

Fig. 8. Current (○), current density (■) (∗) evolution of the AISI 316L electrode immersed in a commercial LiBr solution at 59 mV.

3.4. *Applications of the online visualization technique*

The new technique developed in this paper, including simultaneous electrochemical and image processing analysis, offers the possibility of being used in different areas of the following fields:

(i) *Corrosion:* The online visualization of an electrode surface immersed in a particular medium allows identification of the corrosion mechanism in the system. The versatility of this technique includes the study of different corrosion processes, such as:
- galvanic behaviour of different metallic pairs. This device allows to observe both the anode and the cathode electrodes in these corrosion processes
- failure analysis of a material undergoing pitting corrosion
- study of different protective films such as paints, and metallic coatings, and their degradation; including the analysis of a possible filiform corrosion morphology
- distinction of selective dissolution of one of the components present in an alloy (i.e., dezincification)
- detection of crevice corrosion and/or grain boundary corrosion
- study of inhibitor efficiency
- identification of bubble generation on electrode surfaces
- observation of electrodes which could present exfoliated surfaces during electrochemical tests.

(ii) *Electrowinning:* Direct observation of the growth and morphology of electrodeposited material on the sample surface is possible. Applications include:
- adherence studies of the electrodeposited material
- coating kinetics
- distinction between nucleation and crystal growth.

4. Conclusions

A new methodology has been developed in which not only the electrochemical signal was analysed but also real-time image acquisition which allows determination of the exact corrosion mechanism and the real effect of corrosion on the electrode surface without disturbing the electrochemical system.

The online visualization methodology shows that the uniform corrosion of copper and the different regions of the potentiodynamic curve are closely related to surface changes in the size and appearance of the surface grains.

The polarization curves of copper and stainless steel present similar active regions, with one anodic peak and a following passivation zone; but the images showed that corrosion on the AISI 316L started on the edge of the sample and reached the maximum current when the surface remained completely covered by a reddish film. Copper experienced generalized corrosion from the beginning and its morphology changed homogeneously over the whole surface.

The simultaneous acquisition of images allows elucidation of the origin of the generation of noisy electrochemical signals. In the particular case of AISI 316L, the oscillations observed in the potentiodynamic curve could be related to crevice corrosion between the metallic surface and the Teflon holder.

This new technique, together with image analysis and image processing, is capable of determining the real area through which the measured current is flowing. The exact knowledge of the local current density allows effective prediction of corrosion damage.

Acknowledgements

We wish to thank DGSIC. (convention no. PB97-0336-C02-01) for support of this work. We also acknowledge Dr José Pertusa Grau for his observations on image analysis and Dr M. Asunción Jaime for her translation assistance.

References

1. W. Bogaerts, *Mater. Perform.* **32**(5) (1993) 10–11.
2. S. Journaux, C. Guillaumin, P. Gouton, M. Paindavoine and G. Thauvin, *Opt. Eng.* **38**(8) (1999) 1312–18.
3. P. Fievet, Y. Roques and F. Dabossi, *Critical Factors in Localized Corrosion* 290–298 (The Electrochemical Society, Pennington NJ, 1992).
4. L. Ahuka-Shamba and Y. Roques, *Rev. Met.-CIT* **91**(12) (1994) 1825–33.
5. A. Legat, J. Osredkar and M. Leban, Proc. Exp. Chaos Conference, 4th Meeting (1998) 37–42.
6. S. Lievens, P. Sheunders, G. Van de Wouver, D. Van Dyck, H. Smets, J. Winkelmans and W. Bogaerts, *Microscopy, Microanalysis, Microstructures* **7**(2) (1996) 143–52.
7. S. Lievens, P. Sheunders, G. Van de Wouver and D. Van Dyck, Proc. Workshop Wavelets, Theory and Applications, Leuven, Belgium (May 1996).
8. S. Lievens, P. Sheunders, G. Van de Wouver, D. Van Dyck, H. Smets, J. Winkelmans and W. Bogaerts, *Proceedings of international conference on Computer Analysis of Images and Patterns* (CAIP'95), Lecture notes on computer science, Vol. 970, Prague (Springer-Verlag, 1995), pp. 538–43.

9. J.L. Guiñón, J. García-Antón, V. Pérez-Herranz and G. Lacoste, *Corrosion* **50**(3) (1994) 240–46.
10. J. García-Antón, V. Pérez-Herranz, J.L. Guiñón and G. Lacoste, *Corrosion* **50**(2) (1994) 91–7.
11. A. Igual-Muñoz, J. García-Antón, J.L. Guiñón and V. Pérez-Herranz, 8th Mediterranean Congress of Chemical Engineering, Barcelona (1999).
12. J. García-Antón, M.J. Muñoz, J.L. Guiñón, V. Pérez-Herranz and M.T. Montañés, EUROCORR'99 (European Corrosion Congress), 'Static Corrosion of Copper in an Aqueous Lithium Bromide Solution,' Aachen, Germany (1999).
13. J. García-Antón, M.J. Muñoz, J.L. Guiñón, V. Pérez-Herranz and M.T. Montañés. EUROCORR'99 (European Corrosion Congress), 'Dynamic Corrosion of Copper in an Aqueous Lithium Bromide Solution', Aachen, Germany (1999).
14. A. Igual-Muñoz, J. García-Antón, J.L. Guiñón and V. Pérez-Herranz, EUROCORR'00 (European Corrosion Congress), 'Corrosion Studies of Cu–Ni Alloys in Aqueous Lithium Bromide Solutions', London (2000).
15. J. García-Antón, A. Igual-Muñoz, J.L. Guiñón and V. Pérez-Herranz, Patent P-200002525 (20 Oct. 2000), Spain.
16. J. García-Antón, A. Igual-Muñoz, J.L. Guiñón and V. Pérez-Herranz, Patent P-200002526 (20 Oct. 2000), Spain.
17. Software Visilog 5.2 by NOESIS (1999).
18. J.F. Cooper, R.H. Muller and C.W. Tobias, *J. Electrochem. Soc.* **127** (1980) 1734.
19. T. Aben and D. Tromans, *J. Electrochem. Soc.* **142**(2) (1995) 398–404.
20. N.J. Laycock and R.C. Newman, *Corros. Sci.* **40**(6) (1998) 887–902.
21. P.P. Russell and J. Newman, *J. Electrochem. Soc.* **133** (1986) 59.
22. M.E. Orazem and M.G. Miller, *J. Electrochem. Soc.* **134** (1987) 392.